Density Functional Theory and Conductivity Studi SAND2015-2025J

Boron-Based Anion Receptors

Kevin Leung,* Susan B. Rempe, Mangesh Chaudhari,

Kyle R. Fenton, and Ganesan Nagasubramanian

Sandia National Laboratories, MS 1415, Albuquerque, NM 87185

*kleung@sandia.gov (505)8441588

(Dated: March 6, 2015)

Abstract

Anion receptors that bind strongly to fluoride anions in organic solvents can help dissolve the lithium fluoride discharge products of primary CFx batteries, thereby preventing the clogging of cathode surfaces and improving ion conductivity. They are also potentially beneficial to rechargeable lithium ion and lithium air batteries. We apply Density Functional Theory (DFT) to show that an oxalate-based pentafluorophenyl-boron anion receptor binds as strongly, or more strongly, to fluoride anions than most phenyl-boron anion receptors proposed in the literature. Experimental data shows marked improvement in electrolyte conductivity when this oxalate anion receptor is present. The receptor is sufficiently electrophilic that organic solvent molecules compete with F^- for boron-site binding, and specific solvent effects must be considered when predicting its F^- affinity. To further illustrate the last point, we also perform computational studies on a recently proposed boron ester that exhibits much stronger affinity for both F^- and organic solvent molecules. However, after accounting for specific solvent effects, its net F^- affinity is about the same as the simple oxalate-based anion receptor.

keywords: lithium ion batteries; CFx batteries, density functional theory; computational electrochemistry

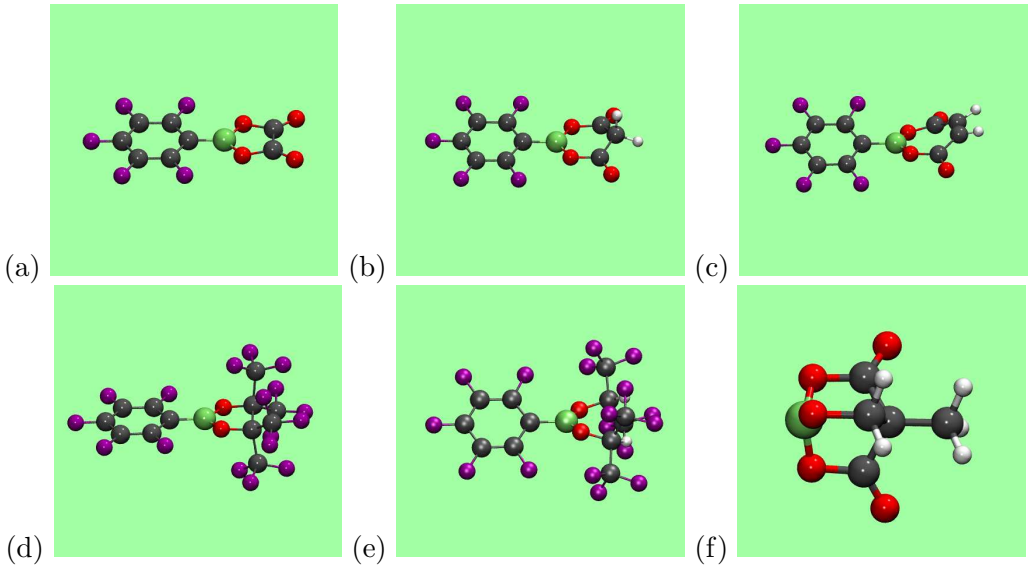

FIG. 1: Optimized structures of (a) ABA0, (b) ABAM, (c) ABA7, (d) ABA12, (e) ABA21, and (f) ABAT. Boron atoms are sp^2 hybridized and reside in planar geometries except in ABAT, where B protrudes slightly out of the plane formed by three O atoms. Grey, red, white, lime green, and purple spheres represent C, O, H, B, and F atoms, respectively. ABA15 is similar to ABA12, but with the CF_3 groups replaced by CH_3.

I. INTRODUCTION

The application of boron-based anion receptors (ABA) in lithium ion and metal-air batteries has been an area of active research.[1–5] Experimental and electronic Density Functional Theory (DFT) studies have been conducted to examine fluoride anion binding affinity, electrolyte conductivity, redox stability, and other properties critical to battery operations. ABAs are particularly useful in primary CFx batteries, where they improve lithium fluoride (LiF) solubility and prevent this discharge product from clogging the cathode surface. Other proposed ABA benefits include F^- scavenging that improves the solid electrolyte interphase (SEI) in lithium ion batteries, and oxygen anion transportation that can improve lithium-air battery charge/discharge reactions.[1]

Boron-based anion receptors often contain strongly electron-withdrawing pentafluorophenyl (C_6F_5) groups. An oft-cited example is tris(pentafluorophenyl)borane (TPFPB).[2] However, ABAs with multiple phenyl groups tend to be bulky molecules, yielding viscous electrolytes that impede ionic motion. In this work, we focus on an oxalate-based "ABA0"

(Figs. 1a and 2a), with the boron atom bound to only one C_6F_5 ring in addition to two oxygen termini of an electron-withdrawing oxalic group.[1] Using electronic structure Density Functional Theory (DFT) techniques, we predict that its gas phase F^- binding free energy is comparable to many higher molecular weight anion receptors that have been examined with computational methods.[5] The gas phase energetics of a subset of ABAs taken from Ref. 5, depicted in Figs. 1 and 2, are re-examined in this work for comparison.

In the presence of liquid solvents, ABA0 binding affinitiy with F^- is found to be even more enhanced compared to other ABA's. Here we apply DFT methods to examine how different ABA's and solvent molecules (S) affect the LiF solvation free energy, according to

$$\mathrm{LiF(solid)} + \mathrm{ABA(solv)} \rightarrow \mathrm{Li^+(solv)} + \mathrm{ABA-F(solv)}. \quad (1)$$

The dissolution process can be broken up into steps of a thermodynamic cycle:

$$\mathrm{LiF(solid)} \rightarrow \mathrm{Li^+} + \mathrm{F^-}; \quad (2)$$

$$\mathrm{Li^+} \rightarrow \mathrm{Li^+(solv)}; \quad (3)$$

$$\mathrm{ABA(solv)} + \mathrm{F^-} \rightarrow \mathrm{ABA-F^-(solv)} \quad (4)$$

In the above equations, "(solv)" denotes solvation by the organic electrolyte; its absence means the species is in the gas phase. Standard states (1.0 M concentration) are assumed for Li^+ and even for the F^- ion considered heuristically to exist in the gas phase. Gas phase contributions to the energetics ultimately cancel in Eqs. 2-4 to recover Eq. 1. The LiF solubility constants in the presence of different ABAs are proportional to the exponentiation of the Eq. 1 reaction free energies. We also present corroborating experimental data that demonstrate the improvement of electrolyte conductivity by ABA0.

Another anion receptor we will highlight in our theoretical studies is a recently proposed constrained boron ester.[3] In traditional ABAs, the B atom exists in a planar, 3-coordinated geometry and exhibits sp^2 hybridization, but becomes sp^3 hybridized when bound to F^- (Fig. 2). The structural changes upon formation of the B-F bond lead to reorganization energy penalties that reduce F^- binding affinity (ΔG_F). By constraining boron in a non-planar geometry even in the absence of F^-, one of the anion receptors of Shanmukaraj *et al.* (Fig. 1f, henceforth referred to as "ABAT") is found to exhibit a gas phase F^- binding affinity that exceeds those of planar boron molecules by more than 1 eV ($\sim$ 23 kcal/mol). Note that we only consider the ABAT monomer, not its dimerized/trimerized complexes.

For strong F^- anion receptors like ABAT, we show that it is crucial to include explicit solvent molecules to predict F^- binding affinity. Consider the following possible intermediate steps toward LiF dissolution implicit in Eq. 1:

$$\mathrm{ABA(solv)} + \mathrm{S\ (solv)} \rightarrow \mathrm{ABA - S\ (solv)} \quad (5)$$

$$\mathrm{ABA(solv)} + \mathrm{F^-} \rightarrow \mathrm{ABA - F^-(solv)} \quad (6)$$

$$\mathrm{ABA - S\ (solv)} + \mathrm{F^-} \rightarrow \mathrm{ABA - F^-(solv)} + \mathrm{S\ (solv)}. \quad (7)$$

"S" is a solvent molecule at its liquid density. Eq. 6 is pertinent to weak anion receptors that do not coordinate to "S." However, the affinities of ABA toward F^- and solvent molecules tend to be correlated: electrophilic anion receptors that bind strongly to F^- also naturally coordinate to organic solvent molecules with nucleophilic oxygen and nitrogen termini. Our work will show that Eq. 5 is thermodynamically favored (downhill) for ABA0 and ABAT. Therefore the exchange reactions of Eq. 7 must be used to predict net F^- binding free energies for these receptors instead of Eq. 6. Such specific solvent binding effects can reduce the selectivity of different ABAs, and can even reverse the ordering, of their F^- binding affinity.

Therefore we also apply DFT methods to survey the interactions of ABAs with four different solvent molecules (Fig. 3): acetonitrile (CH_3CN), dimethyl sulfoxide (C_2H_6SO, DMSO), dimethyl carbonate (C_3H_6O, DMC), and ethylene carbonate ($C_3H_4O_3$, EC). CH_3CN is a standard solvent used for computational benchmarking.[5–7] DMSO is used in synthesis of ABAs (see below). DMC is a co-solvent in standard lithium ion battery electrolyte. Even after subtracting large offsetting ABA-S binding free energies, ABA0 and ABAT are still predicted to be the most thermodynamically favorable F^--binding receptors. In terms of kinetics, strong ABA-solvent interactions may hinder F^- uptake. This is not the focus of our studies. However, we will report experimental evidence of residual ABA-DMSO complexes.

In the theoretical literature, the word "solvent" has been used to describe very different types of solvation models. In the Method section, we distinguish between three treatments of solvation: (1) dielectric continuum; (2) one (or a few) solvent molecules plus dielectric continuum; and (3) explicit treatment of all solvent molecules at finite temperature. In this work, we focus on (2), and highlight its potential qualitative difference with technique (1) which has been used to model anion receptors.[5]

This paper is organized as follows. Section 2 describes the theoretical and experimental

methods used. Section 3 discusses the results, and Section 4 concludes the paper with brief discussions.

II. METHOD

A. Gaussian Suite of Programs

All calculations are conducted using DFT with the PBE0 functional.[8] The Gaussian (G09) suite of programs[9] and a `6-31+G(d,p)` basis are used for geometry optimization of molecular clusters and for computing zero-point-energy (ZPE)/finite temperature corrections. The final, single point energy of each cluster is evaluated using a `6-311++G(3df,2pd)` basis at the optimized geometry.

In Eqs. 5, 6, and 7, "ABA" can be ABA0, ABAM, ABA7, ABA12, ABA15, ABA21, ABAT, and the solvent "S" is one of CH_3CN, DMC, DMSO, and EC. Here the number in ABAX refers to the ordering used in Ref. 5. In Eq. 6, the ABA boron-site is not bonded to the solvent molecule. In contrast, on the right side of Eq. 5 and the left side of Eq. 7 a B-S chemical bond appears. In general, only the one solvent molecule that bonds covalently-with B appears in the calculation, although, in the case of CH_3CN, a larger explicit solvation shell is included as a check.

The polarizable continuum model (PCM)[10] is used to approximate spectator solvent molecules in the outlying bulk electrolyte region surrounding the cluster made up of ABA and solvent molecule(s) in the g09 DFT simulation cell. Various static dielectric constants (ϵ_o) are used to mimic different experimental conditions. Since battery electrolytes typically consist of mixed solvents plus salt, we have applied a ϵ_o=40.0 to the outlying region of all these solvent molecules to mimic a uniform, high-dielectric liquid environment. We also consider pure CH_3CN, DMSO, DMC, and EC solvents, with ϵ_o taken to be 46.7, 35.7, 3.1, and 40.0, respectively. EC is a solid and $\epsilon_o \sim 40$ is adopted to reflect a reasonable value for EC/DMC mixtures. Finally, each CH_3CN, DMSO, EC, DMC, and F^- molecule (at 1.0 M concentration) is assumed to occupy a volume of 86.7, 118, 111, 139, and 1668 $Å^3$, respectively. These values are deduced using their room temperature densities/concentrations, or in the case of EC and DMC, densities at higher/lower temperatures. The volumes lead to slight modifications of default translational entropies reported by the Gaussian suite of pro-

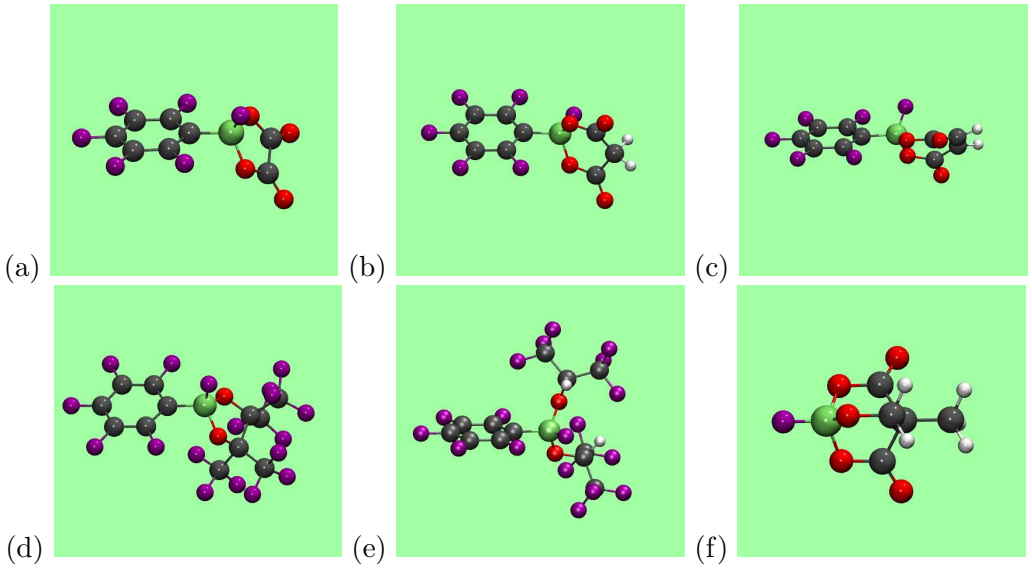

FIG. 2: Optimized structures for (a) ABA0, (b) ABAM, (c) ABA7, (d) ABA12, (e) ABA21, and (f) ABAT bonded to an F^-. Boron atoms are sp^3 hybridized in tetrahedral-like geometries. See Fig. 1 for color key.

grams for 1 atm. standard state reaction gas phase conditions. The corrections contribute less than 0.07 eV to the binding affinities in all cases.

Different organic solvents solvate Li^+ to different extents (Eq. 3), and Li^+ solvation free energies are calculated using Li^+S_4 clusters, with "S"=CH_3CN, EC, DMSO, and DMC. Four explicit solvent molecules are included because Li^+ is generally 4-coordinated in polar solutions. F^- is treated somewhat differently. In most cases, we report results associated with the bare, unsolvated F^-. These unsolvated F^- ions appear only in intermediate steps in the calculations, not the final result (Eq. 1). We justify this treatment because F^- is largely insoluble in organic electrolytes used in batteries; it is expected to exist either as LiF solid or ABA-F, and the free energy of solvated F^- is not needed in most instances. In one case, for the sole purpose of comparing the solubility of LiF in the the absence and presence of ABA, F^- solubility without ABA will be estimated by replacing "ABA (solv)" and "ABA-F (solv)" in the above equations with nothing and "F^- (solv)," respectively. The solvation free energy of F^- herein is computed using a purely dielectric continuum solvation approach at the specified ϵ_o value. A more accurate and consistent way of computing anion solvation free energies is to use one explicit solvation shell of solvent molecules.[11] Our preliminary investigation shows that including more explicit solvents in the calculations only

weakly affects the solvation enthalpy, but it makes the F^- solvation entropy considerably less favorable. Thus the reported LiF solubility in the absence of ABA should be considered an upper limit.

Putting these considerations together, the total solvation reaction free energies ($\Delta G_{\rm diss}$) in Eq. 1 are calculated using either of the following equations,

$$\mathrm{LiF(solid) + ABA(solv) + 4S(solv)} \rightarrow \mathrm{Li^+S_4(solv) + ABA - F(solv)}; \quad (8)$$

$$\mathrm{LiF(solid) + ABA - S(solv) + 3S(solv)} \rightarrow \mathrm{Li^+S_4(solv) + ABA - F(solv)}, \quad (9)$$

depending on whether the ABA in question forms a thermodynamically stable complex with the solvent "S."

B. Different Types of Solvation Models

It is important to distinguish explicit versus implicit solvent treatments in atomistic lengthscale simulations. Most electronic structure (e.g., quantum chemistry or DFT) calculations involve localized basis sets, and a small molecular cluster representing the chemical reaction zone, and relax the geometry of this cluster to its most stable configuration as though it is at zero temperature (T=0 K). The effect of finite temperature is approximated, post-processing, using harmonic expansion to account for vibrational motion and by adding translational/rotational entropies. The outlying region containing liquid solvent is treated implicitly, using dielectric continuum (solvation reaction field) methods.[10] If the reaction zone contains no explicit solvent molecule, the solvation treatment is henceforth described as "type 1."[12] If at least one solvent molecule is included, it is dubbed "type 2."

A more costly approach, which in principle involves less approximations, is *ab initio* molecular dynamics (AIMD, also known as DFT-MD).[13] All atoms, including solute and solvents, are treated at the same DFT level, and periodic boundary conditions are generally applied. The simulation is conducted at finite temperature via solving Newton's equation of motion. This approach ("type 3") avoids the arbitary demarcation of explicit and implicit solvent regions, and is in principle exact given sufficiently large simulation cells, long simulation times, and accurate DFT functionals. In contrast, type 2 solvation exhibits incorrect limiting behavior. When a large number of solvent molecules are included, the nature of the geometry optimization used means that the most stable state of the system should be

a crystallized solid of solvent molecules embedding the solute as an impurity. This clearly does not describe a liquid state configuration. Furthermore, type 2 calculations treat finite temperature effects via harmonic expansion, even when the pertinent solvent motion is diffusive. This approximation can exaggerate the contribution of zero-point energies.

In this work, we will only consider type 1 and type 2 solvation. In most cases, only one explicit solvent molecule is considered. This is reasonable because only one solvent molecule can covalently bond to the boron site. Solvent binding causes extensive geometric changes in most ABAs (Fig. 3). In the ABA literature, to our knowledge, type 1 solvation has been used exclusively.[4] Even such a *purely* continuum approach (type 1) has predicted that the solvent reduces the differential affinity for F^- ($\Delta\Delta G_F$) among different ABA's, defined as the ΔG_F change when switching from one ABA to another, by approximately 25% compared to gas phase $\Delta\Delta G_F$).[4] However, type 1 solvation does not yield the correct geometry changes in ABA (Fig. 3). The present work shows that including an explicit solvent molecule is crucial for strong anion receptors, and can lead to a dramatic modification of F^--binding preference.

C. VASP Calculations

Periodic boundary conditions, planewave-based DFT calculations are applied to compute the zero temperature total energy of LiF solid using the VASP code,[14] PAW pseudopotentials,[15] and the DFT/PBE0 functional.[8] An energy cut-off of 500 eV for plane waves and a 10^{-5} eV wavefunction convergence criterion are enforced. 2-atom FCC cell calculations with 4×4×4 Monkhorst-Pack Brillouin sampling are used to calculate the optimal lattice constant (4.02 Å) and cohesive energy. LiF phonon dispersions are then computed to estimate finite temperature corrections in the harmonic approximation. These are conducted using the same settings, except that a 512-atom (16.08 Å)^3 supercell with Γ-point sampling is applied and the PBE functional is used for this larger simulatnio cell. A finite difference approach is applied to calculate vibrational force constants from this supercell. This yields the dynamical matrix, the eigenvalues of which are vibrational frequencies.[16] The finite temperature correction to the free energy is

$$\Delta G_{\text{harm}} = 1/\beta \sum_i \int_{\mathbf{k}} d\mathbf{k} \log[2\sinh(\beta\hbar\omega_{\mathbf{k},i}/2)]\,, \tag{10}$$

where β is the inverse thermal energy ($1/k_{\mathrm{B}}T$), $\hbar$ is Planck's constant, $\{\mathbf{k}\}$ spans the Brillouin zone, and i is the composite index for the 6 eigenvalues ω of the dynamical matrix at each $\mathbf{k}$-point. Eq. 10 yields a small, 0.067 eV thermal contribution. Therefore we have not pursued improvement to the phonon calculation, e.g., via using the more accurate hybrid PBE0 functional.

D. Experimental Method

Anion binding agents were synthesized using previously reported methods[17] and tested for electrochemical performance. The anion receptors considered include ABA0, ABAM, and a pinacol-based ABA, equivalent to ABA15 considered in Ref. 5. One additional step was executed to remove DMSO from the resulting products. All solids were redissolved in acetone with an excess of LiF. Undissolved LiF was removed by syringe filtration (2 m) and the filtrate condensed by slow evaporation in air. Electrochemical cells were assembled using 2032 coin cells which utilized stainless steel electrodes separated with a polyimide spacer to ensure a uniform electrode separation. The electrolyte is 3:7 (wt %) EC:EMC containing 1.0 M ABA and 1.0 M LiF. Approximately 1 mL of electrolyte for each of the tested binding agents was flooded into the coin cell prior to sealing the cell shut. This was done to ensure that there was complete flooding of the electrochemically accessible area for both electrodes. Conductivity was determined using a Solartron 1287 and 1260 stack by measuring the AC impedance in the frequency range of 100 kHz to 0.1 Hz. The peak-to-peak voltage of the AC signal was limited to 5 mV to avoid any distortion in the response.

X-ray single-crystal data collection was conducted using a Bruker-APEX/CCD diffractometer (Mo Kα, λ=0.71073Å). Indexing and frame integration were performed using the APEX-II software suite. Absorption correction was performed using SADABS (numerical method) also within the APEX-II software. The structures were solved and refined using SHELXS-97 contained in SHELXTL v6.10 packages.

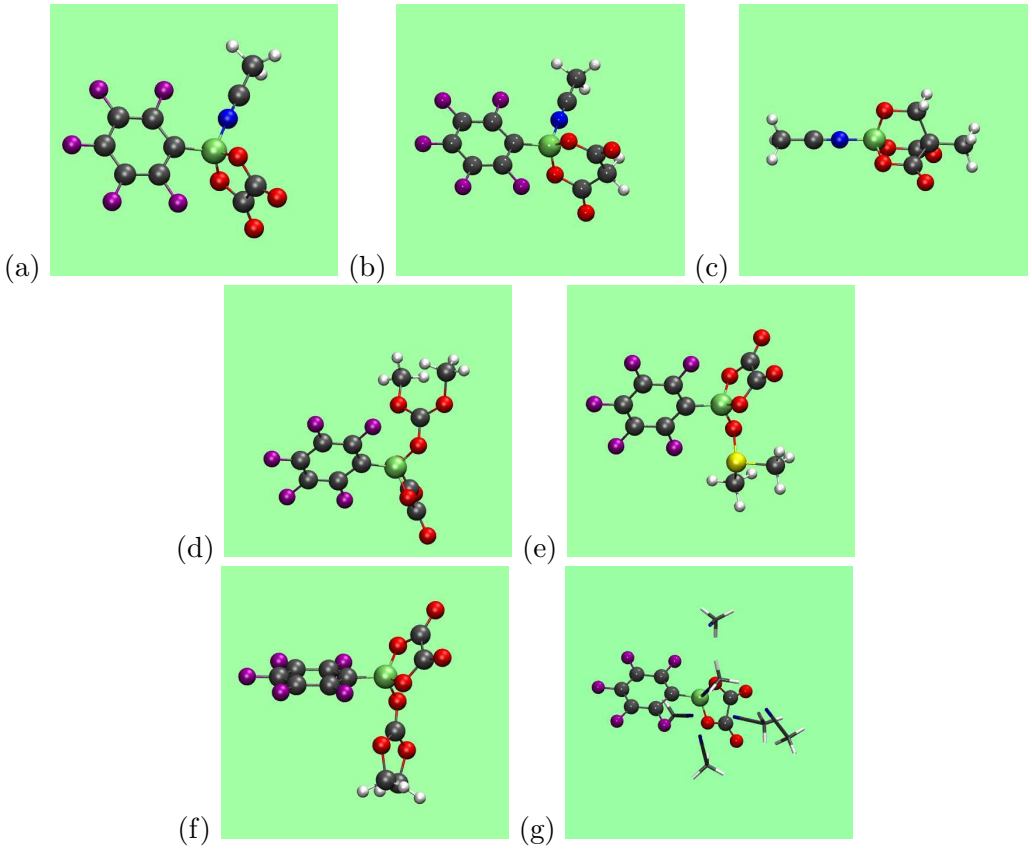

FIG. 3: Optimized structures for (a) ABA0-CH_3CN, (b) ABAM-CH_3CN, (c) ABAT-CH_3CN, (d) ABA0-DMC, (e) ABA0-DMSO, (f) ABA0-EC, and (g) ABA0-$CH_3CN(CH_3CN)_5$. Yellow and blue spheres denote S and N atoms; see Fig. 1 for color key.

III. RESULTS

A. Oxalate and Boron Ester ABA's are Good Anion Receptors

Table I lists new predictions for ABA0, ABAT, and re-examine several fluoride receptors explored in Ref. 5. First we discuss their F^--binding free energies either in vacuum, or with type 1 solvation using a polarizable dielectric continuum (PCM) implicit solvent model (Eq. 6). See the first two rows of Table I. The gas phase binding *enthalpy* (not shown) are comparable to those reported in Ref. 4, although a somewhat different basis set is used compared with that work so as to be compatible with methods used for ABA0 and ABAT herein. For a first estimation of solvation effects, ϵ_o is set to 40 to mimic a generic high dielectric liquid environment. As discussed above, for the purpose of this calculation, F^- is not solvated, and its energetic contribution is constant for all ABAs and solvents.

	ABA0	ABAM	ABA7	ABA12	ABA15	ABA21	ABAT
ABA-F (ϵ_o=1)	-4.351	-4.091	-4.083	-3.914	-2.599	-4.159	-5.366
ABA-F (ϵ_o=40)	-5.917	-5.605	-5.615	-5.405	-4.521	-5.536	-7.193
ABA-S (ϵ_o=40)	-0.157	+0.087	+0.020	NA	NA	+0.055	-1.444
ABA-F*(ϵ_o=40)	-5.760	-5.605	-5.615	-5.405	-4.521	-5.536	-5.749

TABLE I: F- and CH_3CN ("S") binding free energy, computed using Eqs. 5-7. No explicit solvent is present except in the last row, where one CH_3CN is coordinated to the boron site and Eq. 7 (instead of Eq. 6) is used there. ABA12 and ABA15 fails to bind to CH_3CN in the calculations.

In vacuum (first row of Table I), ABA0 binds more strongly to F^- than almost all other ABAs, even those with multiple C_6F_5- electron-withdrawing groups. The exception is ABAT, which is by far the most fluorophilic. As discussed in Sec. 1, ABAT alone has its boron atom in a non-planar geometry in its F^--free state and is less adversely affected by the reorganization energy cost when binding F^-. When the solvent dielectric continuum, *only*, is added (second row of Table I), the $\Delta G_{\rm F}$ ordering remain largely unchanged. It is of interest to compare ABA12 and ABA15, which differ by their two CF_3 and CH_3 groups, only. The electron-withdrawing CF_3 groups lead to a 0.884 eV (20.4 kcal/mol) stabilization of F^- binding for ABA12.

B. Including explicit CH_3CN solvent molecule(s)

Free energies computed using Eq. 6 may overestimate F^--binding in polar solvents because the boron site may bond to solvent molecules. Next we examine the effect of an explicit CH_3CN solvent molecule coordinated to these ABA's (last two rows of Table I). Figs. 3a, b, and c depict the optimized, most enthalpically favorable geometries of ABA-CH_3CN at ϵ_o=40.0. The N-atom terminus of the solvent coordinates to the boron site, just like F^- (Fig. 2), leading to sp^3-hybridization of the B-atom and significant distortion of the molecular geometries compared with unbound ones (Fig. 1a & b). Such distortions are not observed when type 1 solvation treatment is used.

The solvent coordination reactions, ABA0+CH_3CN→ABA0-CH_3CN and ABAM+CN_3CN→ABAM-CH_3CN, exhibit free energy changes of −0.157 and +0.087 eV, respectively. CH_3CN binding to ABA0 is therefore slightly exothermic while it is barely

endothermic for ABAM. Note that the zero temperature binding *enthalpies* to CH_3CN are favorable in both cases: 0.642 and 0.417 eV for ABA0 and ABAM, respectively. As is typical of A + B → C reactions, the translational and rotational entropy penalties add up to more than 0.5 eV. This negates, or almost negates, the substantial favorable reaction enthalpy. As a result, the total free energy value that determines whether a ABA-S complex forms is much smaller than the predicted enthalpies.

Since ABA0 binds to CH_3CN, Eq. 7 should be used. With the explicit solvent contribution added, the F^--affinity (ΔG_F) of ABA0 drops from −5.917 eV to −5.760 eV. ABAM does not bind to CH_3CN, and Eq. 6 should be used. Thus ΔG_F remains −5.605 eV for ABAM (Table I). Inclusion of explicit solvent therefore reduces the differential F^- affinity ($\Delta\Delta G_F$) between ABA0 and ABAM from ∼0.3 eV to ∼0.15 eV, although ABA0 remains a slightly better F^- receptor. ABA7, ABA12, and ABA21 do not bind to CH_3CN, and their ΔG_F also remain unchanged; an explicit CH_3CN should not be present in these models.

ABAT binds strongly to acetonitrile. The free energy associated with Eq. 5 is −1.444 eV (-33.3 kcal/mol). Subtracting Eq. 6 from Eq. 5 yields Eq. 7, from which ΔG_F drastically drops from −7.204 eV to −5.749 eV. In other words, if an explicit CH_3CN is not used in the modeling, the F^--binding affinity would be overestimated by 1.4 eV. This translates into a 2×10^{24}-fold error in the equilibrium constant. With this significant modification due to explicit solvent effects, the F^- affinities of ABA0 and ABAT in CH_3CN become almost identical, despite the large disparity in their gas phase affinities.

We have also considered adding more solvent molecules. Fig. 3h depicts six CH_3CN in the first solvation shell of ABA0, in addition to the use of the PCM dielectric surrounding the explicit solvent region. The F^- binding *enthalpies*, without vibrational corrections, are predicted to be −5.492 and −5.467 eV with one and six CH_3CN, respectively. They are almost identical to each other. However, when thermal and zero-point corrections are included, a larger difference is predicted. This is likely because the additional CH_3CN are only weakly coordinated to the ABA0-CH_3CN complex, but the Gaussian suite of programs treat their weak coordination as harmonic vibrational modes. This can lead to overestimated zero-point energy corrections. Henceforth we only consider one explicit solvent molecule in these calculations.

C. LiF Dissolution

Using the VASP code, the free energy of splitting LiF solid into Li^+ and F^- ions in the gas phase (Eq. 2) is found to be −10.01 eV per formula unit. This includes finite temperature corrections due to solid state vibrational motion at T=300 K (Eq. 10) and the translational entropy gained by Li^+ and F^- corrected to 1.0 M concentration, even though the the ions are assumed to be in gas phase in calculations associated with Eq. 2.

Li^+ solvation properties are needed in dissolution predictions. With a Li^+S_4 cluster and the PCM dielectric continuum approximation outside the cluster, the solvation free energy of Li^+ in CH_3CN is predicted to be −4.747 eV. Incorporating these values into Eq. 9, and using a CH_3CN-specific ϵ_o=35.7 (second column of Table II), the total free energy associated with dissolution of LiF solid in CH_3CN becomes $\Delta G_{\rm diss}$=−0.487 eV. The solubility constant $K_{\rm diss} = \exp(-\beta\Delta G_{\rm diss})\sim 2\times 10^8$, which is much larger than unity In other words, dissolution is favorable. Even though we have not applied the most advanced DFT functionals,[18] the uncertainty of the computational method is unlikely to exceed 0.4 eV, which suggests that the $K_{\rm diss} >> 1$ conclusion should lie within the margin of error. Using similar calculations, ABAM and ABAT are predicted to yield LiF free energy more negative than the −10.01 eV of Eq. 2. Therefore $K_{\rm diss} >> 1$ and LiF are soluble in the presence of these ABA's.

In the absence of any ABA, a purely dielectric continuum ("type 1") treatment of of F^- solvation yields −3.664 eV at 1.0 M F^- concentration. Compared with the last row of Table I, it is clear that all ABAs binds to F^- far more favorably than the "solvent" by itself. Thus boron based anion receptors exhibit a dramatic effect on LiF dissolution. Indeed, without ABA, $K_{\rm diss}$ drops to 2×10^{-30}, and LiF should be largely insoluble. We stress that we do not consider charge-neutral, Li-F contact ion dimers, only well-separated Li^+ and F^- ions which contribute to electrolyte conductivity.

D. Survey of Other Solvent Molecules, with ABA0, ABAM, and ABAT

DMSO is used during our synthesis of ABA0, and it exhibits the highest ABA-binding free energies among solvents examined in this work (Table II). Figure 4 depicts the X-ray crystal structure of ABA0-DMSO prior to solvent exchange, and after DMSO is replaced by F^-. The before-exchange picture clearly demonstrates that the boron site becomes sp^3

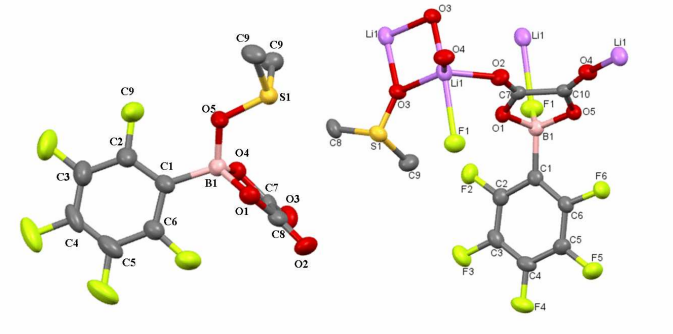

FIG. 4: X-ray crystal structures of ABA0-DMSO prior to solvent exchange, and ABA0-F^- after solvent exchange. The color scheme used is slightly different from Figs. 1-3. F, B, and Li are in green, light pink, and dark pink instead of purple, dark green, and dark blue. Protons are subsumed into carbon atoms.

hybridized due to formation of a covalent bond with the oxygen of the DMSO molecule. The predicted structure (Fig. 3f) looks similar, except that the DMSO molecule is rotated so that one of its CH_3 protons coordinates to an F^- on the phenyl ring. Since the calculation only contains one ABA0-DMSO complex and omits the surrounding molecules to which DMSO can coordinate in X-ray spectrum sample, the difference is understandable. Table II shows that, at room temperature, both ABA0-DMSO and ABAM-DMSO complexes are favorable. Even after subtracting the free energy cost of breaking the ABA-DMSO bond to form ABA-F (i.e., using Eq. 7 rather than Eq. 6), ABA0 retains a slight preference for F^--binding relative to ABAM in DMSO, while ABAT is slightly inferior to both by $\sim$0.1 eV.

Other solvents like DMC, and EC have smaller specific solvent effects (Table II). They exhibit unfavorable binding free energies with ABAM. Therefore ABAM should retain its planar geometry, and type 1 dielectric continuum calculations suffice for this ABA. In contrast, ABA0 binds to all these solvent molecules, albeit marginally. ABAT exhibits substantial binding free energies to all solvents. After subtracting its solvent binding free energies, this ABA is predicted to be slightly inferior to ABA0 for binding F^- in all cases.

The choice of solvent molecules affect not only ABA-F binding, but also the Li^+ solvation free energy (Eqs. 3, 8, and/or 9), and in turn, the LiF solubility constant. Li^+ solvation free energies in CH_3CN, DMSO, DMC, and EC are -4.746, -5.008, -2.195, and -4.445, respectively, when computed at the respective ϵ_o of the pure solvent (Table II). Adding $\Delta G_{\rm F}$

	CH_3CN	DMSO	DMC	EC
ϵ_o	35.7	46.7	3.1	40.0
ABA0-F	-5.903	-5.923	-5.451	-5.903
ABAM-F	-5.592	-5.608	+3.291	-5.592
ABAT-F	-7.187	-7.200	-6.627	-7.193
ABA0-S	-0.159	-0.602	-0.124	-0.038
ABAM-S	+0.086	-0.330	+0.078	+0.168
ABAT-S	-1.443	-1.975	-1.239	-1.365
ABA0-F*	-5.744	-5.321	-5.327	-5.865
ABAM-F*	-5.592	-5.276	+3.291	-5.592
ABAT-F*	-5.744	-5.225	-5.388	-5.828
Li^+S_4	-4.746	-5.008	-2.195	-4.445
ABA0-F/Li^+	-10.490	-10.329	-7.522	-10.310
ABAM-F/Li^+	-10.338	-10.014	-1.096	-10.037
ABAT-F/Li^+	-10.490	-10.233	-7.583	-10.273

TABLE II: F^-- (ABA-F) and solvent-binding (ABA-S) free energies, Li^+ solvation free energies computed with an explicit solvent shell of 4 molecules (Li^+S_4), and sum of these two (ABA-F/Li^+), in eV. In the case of F^-, the asterisk refers to the correct binding free energies (Eq. 7) if the ABA binds to the solvent molecule (i.e., Eq. 6 yields an attractive free energy). The ABA15-F/Li^+ value in EC solvent ($\epsilon_o = 40$) is -8.966 eV.

to Li^+ solvation free energies from Table II to yield $\Delta G_{\rm diss}$ (Eq. 8 or 9) and comparing with -10.01 eV from Eq. 2, we find that LiF is marginally soluble in 1.0 M ABA0 in the presence of CH_3CN, DMSO, and EC. With ABAM, LiF is soluble in CH_3CN; its solubility in DMSO and EC are within the margins of computational uncertainties. We have also considered ABA15. The boron site of this anion receptor does not bind to either EC or CH_3CN. To compare with measurements in EC/DMC mixture (see below), $\epsilon_o = 40$ is applied. Li^+ solvation free energy in EC and ABA15-F binding free energies add to -8.966 eV, which is much less favorable than the -10.01 eV LiF solid cohesive free energy. Hence ABA15 is not expected to dissolve LiF solid.

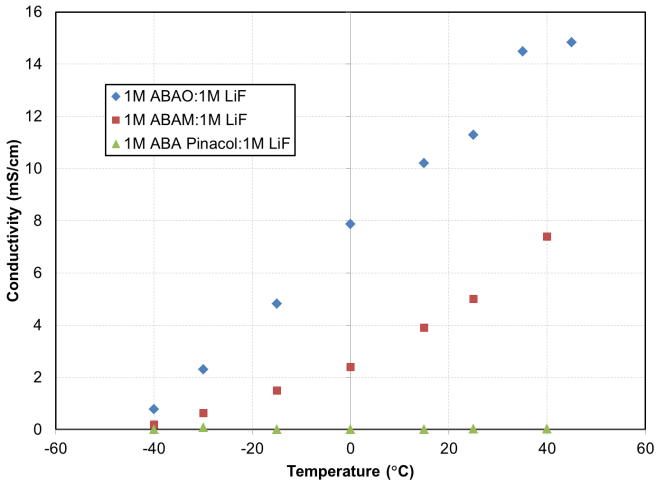

FIG. 5: Electrolyte conductivity. Blue, red, and green represent 1.0 M ABA0, ABAM, and ABA15 in the electrolyte, respectively.

E. Conductivity Measurements

Fig. 5 depicts the electrolyte conductivity measured in the coin cells as a function of temperature. ABA0 exhibits the highest conductivity at all temperatures, while ABAM is a factor of 2-3 lower. The conductivity in ABA15 is negligable. At least two factors contribute to mobility: the ability to dissolve LiF and the intrinsic viscosity. The ABA15-containing does not accommodate the 1.0 M LiF salt; most of the salt precipates out. This is mainly responsible for its low conductivity. These results are consistent with the theoretical predictions that ABA0 readily dissolves LiF, ABAM is slightly inferior, while LiF is hardly soluble in electrolyte with ABA15.

IV. CONCLUSIONS

Using both DFT predictions and conductivity measurements, we have shown that ABA0 is a promising fluoride receptor. After accounting for explicit solvent effect, the equilibrium constant K for the reaction

$$\text{ABA0(solv)} + \text{LiF(solid)} \rightarrow \text{ABA0} - \text{F}^{-}\text{(solv)} + \text{Li}^{+}\text{(solv)}$$

is the largest among ABA's. Its K even slightly exceeds that of a recently proposed ABAT with the boron atom in a non-planar environment[3] when specific solvent effects are taken

into account. Indeed, for these strong F^--binding anion receptors, it is found that including explicit ABA-S covalent bonding for different choices of solvent is crucial. Omitting the solvent molecule in the calculations can lead to binding coefficients that are in error by many orders of magnitude.

Acknowledgement

Sandia National Laboratories is a multiprogram laboratory managed and operated by Sandia Corporation, a wholly owned subsidiary of Lockheed Martin Corporation, for the U.S. Deparment of Energy's National Nuclear Security Administration under contract DE-AC04-94AL85000.

[1] See, for a review, Reddy, V.P.; Blanco, M.; Bugga, R. Boron-based Anion eceptors in Lithium-ion and Metal-air Batteries. *J. Power Sources* **2014**, *247*, 813-820.

[2] Nair, N.G.; Blanco, M.; West, W.; Weise, F.C.; Greenbaum, S.; Reddy, V.P. Fluorinated Brooxin-Based Anion Receptors for Lithium Ion Batteries: Fluoride Anion Bind, Ab Initio Calculations, and Ionic Conductivity Studies. *J. Phys. Chem. A* **2010**, *132*, 3055-3062

[3] Shanmukaraj, D.; Grugeon, S.; Gachot, G.; Laruelle, S.; Mathiron, D.; Tarasocon, J.-M.; Armand, M. Boron Esters and Tunable Anion Carriers for Non-Aqueous Batteries Electrochemistry. *J. Am. Chem. Soc.* **2010**, *132*, 3055-3062

[4] Qin, Y.; Chen, Z.; Lee, H.S.; Yang, X.-Q.; Amine, K. Effect of Anion Receptor Additives on Electrochemical Performance of Lithium-ion Batteries. *J. Phys. Chem. C* **2010**, *114*, 15202-15206

[5] Chen, Z.; Amine, K. Computational Estimates of Fluoride Affinity of Boron-Based Anion Receptors. *J. Electrochem. Soc.* **2009**, *156*, A672-676.

[6] Han, S.D.; Borodin, O.; Seo, D.M.; Zhou, S.B.; Henderson, W.A. Electrolyte Solvation and Ionic Association V. Acetonitrile-Lithiu Bis(fluorosulfonyl)imide (LiFSI) Mixtures. *J. Electrochem. Soc.* **2014**, *161*, A2042-2053.

[7] Sodeyama, K.; Yamada, Y.; Aikawa K.; Yamada, A.; Tateyama, Y. Sacrificial Anion Reduction Mechanism for Electrochemical Stability Improvement in Highly Concentrated Li-Salt Electrolyte. *J. Phys. Chem. C* **2014**, *118*, 14091-14097.

[8] Adamo, C.; Barone, V. Towards reliable density functional methods without adjustable parameters: the PBE0 model. *J. Chem. Phys.* **1999**, *110*, 6158-6169.

[9] Gaussian 09, Revision A.1, Fritsch, M.J.; *et al.*, Gaussian, Inc., Wallingford CT, 2009.

[10] Sealmani, G.; Frisch, M.J. *J. Chem. Phys.* **2010**, *132*, 114110.

[11] Brayantsev, V.S. Calculation of solvation free energies of Li^+ and O_2^- ions and neutral lithium-oxygen compounds in acetonitrile using mixed cluster/continuum models. *Theor. Chem. Acc.* **2012**, *131*, 1250-1257.

[12] See, e.g., Tasaki, K.; Harris, S.J. Computational Study on the Solubility of Lithium Salts Formed on Lithium Ion Battery Negative Electrode in Organic Solvents. *J. Phys. Chem. C* **2010**, *114*, 8076-8083.

[13] CPMD Version 3.4, J. Hütter, P. Ballone, M. Bernasconi, P. focher, E. Fois, S. Goedecker, D. Marx, M. Parrinello, and M. Tuckerman, MPI für Festkörperforschung and IBM Research Laboratory (1990-1998), Copyright IBM 1990, 1997, Copyright MPI 1997.

[14] Kresse, G.; Furthmüller, J. Efficienct Iterative Schemes for Ab Initio Total-Energy Calculations Using a Plane-wave Basis Set. *Phys. Rev. B* **1996**, *54*, 11169.

[15] Kresse, G.; Joubert, J. From Ultrasoft Pseudopotentials to the Porjector Augmented-Wave Method. *Phys. Rev. B* **1999**, *59*, 1758-1775.

[16] Giannozzi, P.; de Gironcoli, S.; Pavone, P.; Baroni, S. *Ab initio* Calculation of Phonon Dispersions in Semiconductors. *Phys. Rev. B* **1991**, *43*, 7231-7241.

[17] Li, L.F.; Xie, B.; Lee, H.S.; Li, H.; Yang, X.Q.; McBreen, J.; Huang, X.J. Studies on the Enhancement of Solid Electrolute Interphase formation on Graphitized Anodes in Li-X-carbonate based Electrolytes using Lewis Aid Additives for Lithium-ion Batteries. *J Power Sources*, **2009**, *189*, 539-542.

[18] For a comparison of high-level quantum chemistry and DFT calculations, see Borodin, O.; Smith, G.D. Quantum Chemistry and Molecular Dynamics Simulation Study of Dimethyl Carbonate: Ethylene Carbonate Electrolytes Doped with $LiPF_6$. *J. Phys. Chem. B* **2009**, *113*, 1763-1776.

[19] Yanase, S.; Oi, T. Solvation of Lithium Ion in Organic Electrolyte Solutions and Its Isotopie Reduced Partition Function Ratios Studied by ab initio Molecular Orbital Method. *Journal of Nuclear Science and Technology*, **2002**, 39, 1060-1064.

[20] Leung, K.; Tenney, C.M. Towards First Principles Prediction of Voltage Dependences of Electrode/Electrolyte Interfacial Processes in Lithium Ion Batteries. *J. Phys. Chem. C* **2013**, *117*, 24224-24235.

[21] Perdew, J.P.; Burke, K.; Ernzerhof, M. Generalized Gradient Approximation Made Simple. *Phys. Rev. Lett.* **1996**, *77*, 3865-3868.

[22] Pratt, L.R. Contact Potentials of Solution Interfaces: Phase Equilibrium and Interfacial Electric Fields. *J. Phys. Chem.* **1992**, *96*, 25-33.

[23] Leung, K. Surface Potential at the Air-Water Interface Computed Using Density Functional Theory. *J. Phys. Chem. Lett.* **2010**, *1*, 496-499.